Parametric x radiation from thick crystals

I. Endo, M. Harada, T. Kobayashi, Y.S. Lee, T. Ohgaki, and T. Takahashi*
Faculty of Science, Hiroshima University, Kagamiyama, Higashi-Hiroshima 724, Japan

M. Muto and K. Yoshida
Institute for Nuclear Study, University of Tokyo, Tanashi, Tokyo 188, Japan

H. Nitta
Department of Physics, Tokyo Gakugei University, Koganei, Tokyo 184, Japan

A.P. Potylitsin, and V.N. Zabaev
Nuclear Physics Institute, Tomsk Polytechnical University, 634050, Tomsk, Russia

T. Ohba
Department of Materials Science and Engineering, Teikyo University Utsunomiya, 320, Japan

(Received 25 October 1994)

The parametric x radiation from thick Si single crystals with 0.5–5 mm thickness was investigated at an electron energy of 900 MeV. As the crystal thickness increased, both intensity and angular spread reached a plateau after their increase in the thin crystal region, resulting in more brilliant x ray's than the Feranchuk and Ivashin's prediction [J. Phys. (Paris) **46**, 1981 (1985)] for thick crystals. This behavior is consistent with the incoherent model proposed in our previous paper [Phys. Rev. Lett. **70**, 3247 (1993)].

PACS number(s): 42.25.Fx, 78.90.+t

When relativistic particles pass through crystals, an intense and monocromatic x ray is emitted into the Bragg angle as if the crystal were irradiated by x ray instead of particles. This phenomenon, known as parametric x radiation (PXR), can be interpreted as Bragg diffraction of virtual photons associated with incident particles. The PXR has been attracting much attention since it is, with an electron linear accelerator of modest size, a candidate for a monochromatic and high-brilliance x-ray source of continuously tunable wavelengths [1,2].

Experimental and theoretical works have shown that most of the qualitative natures of PXR are well accounted for by kinematic theory [3–12]. However, a quantitative description of the phenomenon is yet to be studied. In fact, recent papers pointed out that the effects of multiple scattering as well as mosaicity of the crystal were not explained by existing theories [13,14]. From a practical point of view, it is important to know to what extent the crystal thickness can be increased without deteriorating the x-ray quality. It is to be recalled that the Feranchuk-Ivashin (FI) model [15] predicts a drastic decrease of the intensity and an increase of the angular spread of the PXR due to the electron multiple scattering in thick crystals. The purpose of this experiment is to investigate the effect of electron multiple scattering by observing the thickness dependence of the PXR in the region where the crystal is thicker than its x-ray absorption length.

The experiment was performed at the 1.3-GeV electron synchrotron at the Institute for Nuclear Study, University of Tokyo. The electron energy was 900 MeV. The experimental setup is shown in Fig. 1. The target crystals were 20×20 mm^2 monocrystalline silicon plates and their thicknesses were 0.20, 0.50, 1.0, 1.5, 2.0, and 5.0 mm. The surfaces of the plate and one of the edges were normal to the crystallographic axes $[\bar{1}11]$ and [110], respectively. The $[\bar{1}1\bar{2}]$ axis was vertically aligned and the (110) plane was used as a reflection plane. The crystal was mounted on a three-axis computer-controlled goniometer whose angular resolution was 0.004°. A NaI scintillation counter was used as an x-ray spectrometer, which was placed at two different positions as described later. The signal from the NaI detector was fed into a single channel analyzer (SCA) and the number of signals in between two discrimination levels was counted by a scalar. The discrimination levels of the SCA was chosen to pick up signals from either (220) or (440) reflection. The number of electrons passing through the target crystal was monitored by a thick-walled ionization chamber placed downstream of the target crystal. The intensity of the electron beam was approximately 10^7 s^{-1} during the experiment. The electron beam extracted from the vacuum chamber of the synchrotron reached the target through the exit window of the vacuum chamber of 125-

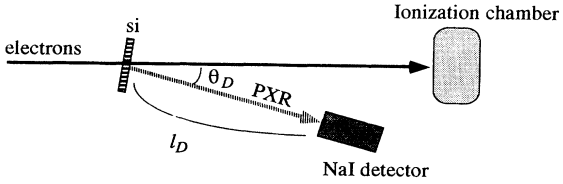

FIG. 1. Experimental setup.

μm-thick Mylar followed by 39.8 cm of air. The size and the angular spread of the incident electron beam, including multiple scattering in the air and the window of the vacuum chamber, were 0.8 mm and 0.5 mrad in a standard deviation, respectively.

The PXR was measured in a Laue geometry at two different positions, i.e., the far position $\theta_D = 24.8°$, $l_D = 753$ cm and the near position $\theta_D = 19.0°$, $l_D = 193$ cm, where θ_D is the x-ray detection angle with respect to the electron beam axis and l_D is the distance between the crystal and the detector. The data taken at the far position were sensitive to the intrinsic angular divergence of PXR, because the effect of the finite angular coverage of the NaI detector and the spatial distribution of the incident electron beam were small. On the other hand, data at the near position were suited for the intensity measurement thanks to its insensitivity to the angular divergence of the PXR and the detector coverage.

An x-ray energy spectrum taken at the near position with the 0.2-mm-thick crystal is shown in Fig. 2. Clear peaks for the (220) and the (440) reflections were observed. The peak energies of 20.3 and 39.2 keV obtained by Gaussian fitting after background subtraction were consistent with the expected values. The hatched areas 1 and 2 in Fig. 2 are the regions in which photons were regarded as belonging to the (220) and the (440) reflections, respectively.

A PXR intensity as a function of angle θ is shown in Fig. 3, where θ is the rotation angle around the vertical axis. The curve in the figure is the fit to the data with the following expression:

$$N(\theta) = M\frac{\theta_a^2(\theta-\theta_B)^2+\theta_W^4}{\{(\theta-\theta_B)^2+\theta_W^2\}^2}+B, \qquad (1)$$

where $N(\theta)$ is the number of counts in each reflection defined in Fig. 2 and $\theta_B = \frac{1}{2}\theta_D$ is the Bragg angle. M, θ_W, θ_a, and B are fitting parameters. M is the peak height after subtraction of the constant background B. θ_W and θ_a are parameters related to the width and the shape of the peak. The full width at half the maximum (FWHM) of the angular distribution of the PXR is obtained from the fitted parameters as

$$\theta_{\mathrm{FWHM}} = 2\sqrt{(\theta_a^2-\theta_W^2)+\sqrt{(\theta_a^2-\theta_W^2)^2+\theta_W^4}}.$$

The width of the angular distribution of the PXR can be expressed in the form

$$\theta_{\mathrm{FWHM}}^2 = (1+\sqrt{2})^2\theta_{\mathrm{ph}}^2+\theta_{\mathrm{acc}}^2,$$

where θ_{acc} is the contribution from the detector acceptance and was 2 and 8 mrad for the far and the near positions, respectively. θ_{ph} is the angular width of the PXR and can be expressed by kinematic theory [15] as

$$\theta_{\mathrm{ph}}^2 = \frac{1}{\gamma^2}+\theta_{\mathrm{MS}}^2+\left(\frac{\omega_p}{\omega}\right)^2, \qquad (2)$$

where γ, ω_p, and ω are the Lorenz factor of the incident electron, the plasma energy of silicon, and the x-ray energy, respectively. The contribution from the multiple scattering of the incident electron is represented by θ_{MS}. The width parameter θ_{FWHM} for (220) and (440) reflections obtained at the far position are plotted as a function of crystal thickness in Fig. 4. It was shown that the width for (440) was appreciably narrower than that for (220) at any crystal thickness, which indicated that the ω_p/ω term dominated in (2). The data showed that the width of the PXR did not keep increasing with crystal thickness but saturated at 2 mm for the (220) reflection, which was in contrast to the FI model prediction, as demonstrated by the solid and the dashed lines in the figure. Also shown in Fig. 4 is the Monte Carlo simulation by the incoherent model proposed in our previous paper [13] in which the electron multiple scattering was

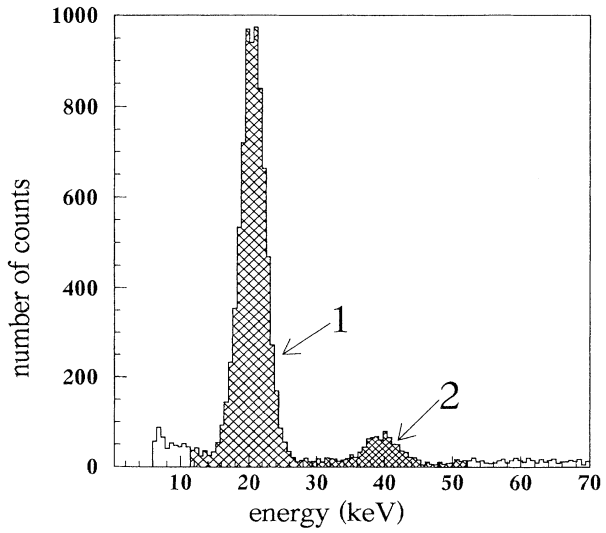

FIG. 2. PXR spectrum obtained with the crystal thickness 0.2 mm at $E_e = 900$ MeV in the near position. Hatched areas 1 and 2 define (220) and (440) reflections, respectively.

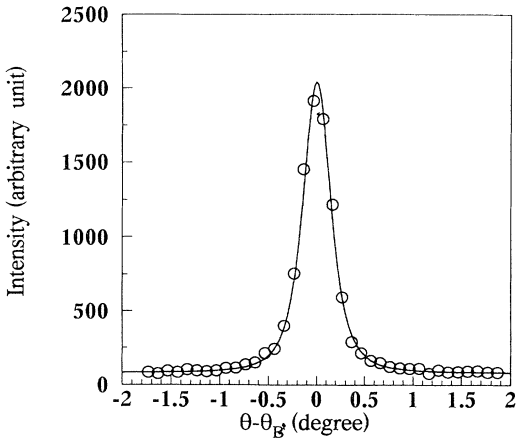

FIG. 3. Crystal angle dependence of PXR intensity from the (220) (circles) reflection at the far position. The curve is the best fit to expression (1) in the text. The crystal thickness is 1.0 mm.

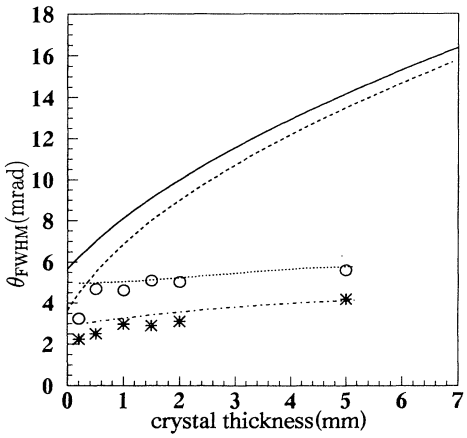

FIG. 4. Crystal thickness dependence of the width parameter θ_{FWHM}. The circles are for (220) and the asterisks are for (440). The solid and the dashed lines are predictions of the FI model for (220) and (440) reflections. The dotted and the dot-dashed lines are the Monte Carlo simulation by the incoherent model (see text) for (220) and (440) reflections, respectively.

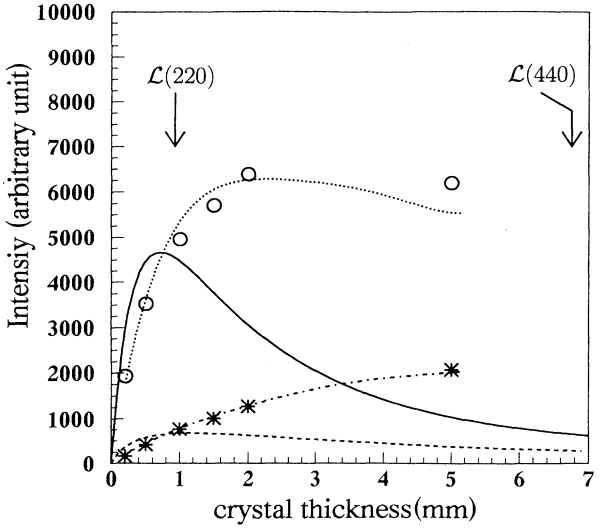

FIG. 5. Crystal thickness dependence of the PXR intensity. The circles are for (220) and the asterisks are for (440). The solid and the dashed lines are predictions of the FI model for (220) and (440) reflections. The dotted and the dot-dashed lines are the Monte Carlo simulation by the incoherent model for (220) and (440) reflections. The arrows show the x-ray absorption length ($\mathcal{L}$) in the crystal for (220) and (440) reflections, respectively.

taken into account by smearing the direction of incident electrons in the simulation with θ_{MS} in (2) being set to 0. The incoherent model showed good agreement with the data except for the 0.2 mm thickness. The discrepancy between the data and the FI model can be attributed to the treatment of the effect of the multiple scattering since θ_{MS} in the FI model is a simple increasing function of the crystal thickness.

The thickness dependence of the PXR intensity, measured at the near position, is shown in Fig. 5. The FI prediction did not reproduce the intensity data either; it decreased too rapidly with the crystal thickness. The reason can be attributed to the improper treatment of the multiple scattering, as indicated in the width analysis. The intensity of the PXR can be described as

$$I(L) = A(1 - e^{-\frac{L}{\mathcal{L}}})\left[\ln\left(\frac{\theta_{\mathrm{acc}}^2 + \theta_{\mathrm{ph}}^2}{\theta_{\mathrm{ph}}^2}\right) - \frac{\theta_{\mathrm{acc}}^2}{\theta_{\mathrm{acc}}^2 + \theta_{\mathrm{ph}}^2}\right], \quad (3)$$

where $I(L)$ is the PXR intensity, A is the normalization factor to be fitted, and $\mathcal{L}$ is the x-ray absorption length. In this expression, the crystal-thickness (L) dependence is in the θ_{FWHM} term through the electron multiple scattering effect as well as in the photon absorption part $(1 - e^{-\frac{L}{\mathcal{L}}})$. The decrease of the PXR intensity for thick crystals in the FI model is due to too much expansion of θ_{ph}, as seen in the width analysis. The incoherent model is also plotted in Fig. 5 and fairly good agreement between the model and the data is seen.

We measured the intensity and the angular spread of the PXR from thick silicon crystal. It was found that the intensity of the PXR did not decrease as the crystal thickness increased, but reached some saturated value. We also found that the angular spread of the PXR did not keep increasing with crystal thickness either. This observation was contrary to the prediction of the FI model. The model based on the incoherent treatment of the electron multiple scattering effect agreed with the data in thick crystal region. In the thin region, the angular spread of the PXR was narrower than in the incoherent model, particularly at the 0.2 mm thickness. This indicates that another treatment of the electron multiple scattering is required in the thin region, assuming that the data at 0.2 mm is not invalidated by unknown instrumental error. Anyway, a more systematic investigation is necessary in thin region where the data can be compared with the more sophisticated model developed by Baryshevsky *et al.* [3].

The authors would like to thank the electron sycrotron operation crew of INS for supplying excellent beams during the experiment. This work was supported in part by Mitsubishi Foundation.

* Corresponding author. Electronic address: takahasi@photon.hepl.hiroshima-u.ac.jp

[1] V.G. Baryshevsky and I.D. Feranchuk, Nucl. Instrum. Methods **228**, 490 (1985).

[2] R.B. Fiorito *et al.*, Proceedings of 12th International Conference on the Applications of Accelerators in Research and Industry, Denton, 1992 [Nucl. Instrum. Methods B **79**, 758 (1993)].

[3] V.G. Baryshevsky, A.O. Grubich, and Le Tien Hai, Zh. Eksp. Teor. Fiz. **94**, 51 (1988) [Sov. Phys. JETP **67**, 895

(1988)].
[4] H. Nitta, Phys. Lett. A **158**, 270 (1991).
[5] H. Nitta, Phys. Rev. B **45**, 7621 (1992).
[6] A. Caticha, Phys. Rev. B **45**, 9541 (1992).
[7] S.A. Vorob'ev, B.N. Kalinin, S. Pak, and A.P. Potylitsyn, Pis'ma Zh. Eksp. Teor. Fiz. **41**, 3 (1985) [JETP Lett. **41**, 1 (1985)].
[8] Yu.N. Adishchev *et al.*, Nucl. Instrum. Methods B **44**, 130 (1989).
[9] A.V. Shchagin, V.I. Pristupa, and N.A. Khizhnyak, Phys. Lett. A **148**, 485 (1990).
[10] Yu.N. Adishchev *et al.*, Phys. Lett. A **147**, 326 (1990).
[11] K.Yu. Amosov *et al.*, Phys. Rev. E **47**, 2207 (1993).
[12] Yu.N. Adishchev *et al.*, Nucl. Instrum. Methods B **21**, 49 (1987).
[13] S. Asano *et al.*, Phys. Rev. Lett. **70**, 3247 (1993).
[14] R.B Fiorito *et al.*, Phys. Rev. Lett. **71**, 704 (1993).
[15] I.D. Feranchuk and A.V. Ivashin, J. Phys. (Paris) **46**, 1981 (1985).

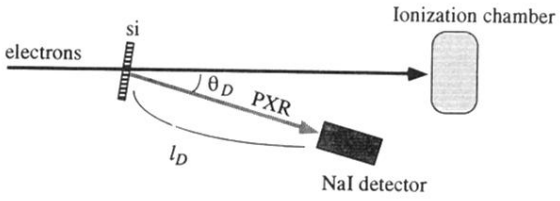

FIG. 1. Experimental setup.